Radioluminescent Light Source for the Development of Optical Sensor Arrays

ARTICLE *in* ANALYTICAL CHEMISTRY · FEBRUARY 2005

Impact Factor: 5.64 · DOI: 10.1021/ac048985g · Source: PubMed

6 AUTHORS, INCLUDING:

Elizabeth C Tehan

18 PUBLICATIONS **383** CITATIONS

SEE PROFILE

Rachel M Bukowski

University at Buffalo, The State University of…

16 PUBLICATIONS **297** CITATIONS

SEE PROFILE

Nigel J Kent

Dublin City University

21 PUBLICATIONS **196** CITATIONS

SEE PROFILE

Brian D Maccraith

Dublin City University

186 PUBLICATIONS **5,201** CITATIONS

SEE PROFILE

Anal. Chem. **2005,** *77,* 718−723

Radioluminescent Light Source for the Development of Optical Sensor Arrays

William G. Holthoff,[†] Elizabeth C. Tehan,[†] Rachel M. Bukowski,[†] Nigel Kent,[‡] Brian D. MacCraith,*[,‡] and Frank V. Bright*[,†]

Department of Chemistry, Natural Sciences Complex, University at Buffalo, The State University of New York, Buffalo, New York 14260-3000, and National Centre for Sensor Research, Dublin City University, Glasnevin, Dublin 9, Ireland

A radioluminescent (RL) light source is evaluated for the development of photonically based chemical-responsive sensor arrays (CRSAs). The RL light source is comprised of a strontium-90 (^{90}Sr) radionuclide and a plastic scintillator. The β particles emitted from the ^{90}Sr generate blue light (λ_{max} = 435 nm) from the plastic scintillator, and the blue light excites the analyte-responsive luminophores within the CRSA. To assess the RL light source utility, we have determined the analytical figures of merit from two tris(4,7′-diphenyl-1,10′-phenathroline)ruthenium-(II)-doped xerogel-based sensor platforms: (i) a planar 5 × 5 multielement array and (ii) a discrete sensor element formed on the proximal face of poly(styrene) pillars that have a frustrated cone (frustum) geometry. We compare the performance from each platform when it is excited by a He−Cd laser (442 nm), a blue light-emitting diode (460−470 nm), and the RL light source. The RL light source yields results that are statistically equivalent to results from either electrically powered light source. The RL light source consumes no electrical power, is compact and simple, and has an extremely stable time-averaged signal. The primary trade-offs for these advantages are the RL light source's lower radiant power and the corresponding longer data acquisition times.

Substantial effort has been expended to develop chemical sensor platforms with an eye toward "remote sensing" and long-term deployment.[1−3] In these systems an overarching factor that governs what one can do with such a sensor platform is the amount of available power. Thus, although batteries,[4] solar conversion systems,[5] and energy harvesters[6,7] are becoming more efficient and lighter in weight, available power is still the primary limitation for long-term sensor deployment in remote locations. Over the past few years, our research groups have focused on developing photonically based sensors and arrays that are small in size and that consume minimal electrical power. These systems have been based on the combination of new xerogel-based sensor elements,[8−11] ultrastable pin-printed chemical sensor arrays (PPCSAs),[12−15] novel complementary metal oxide semiconductor (CMOS) array detectors,[16] light-emitting diode (LED) light sources,[15−17] and higher efficiency light collection geometries (e.g., frustrated cones).[18,19] To reduce power demands further, we explore a radioluminescent (RL) light source as a "no power" alternative to the LED.

The use of an RL light source for photometric measurements is not new.[20−40] For example, RL light sources have been used in

* To whom correspondence should be addressed. (F.V.B.) Phone: (716) 645-6800, ext. 2162. Fax: (716) 645-6963. E-mail: chefvb@acsu.buffalo.edu. (B.D.M.) Phone: 353-1-700-5299. Fax: 353-1-700-8021/8484. E-mail: Brian.MacCraith@dcu.ie.

† University at Buffalo, The State University of New York.

‡ Dublin City University.

(1) Narayanaswamy, R.; Wolfbeis, O. S. *Optical sensors: industrial, environmental and diagnostic applications*; Springer: Berlin, London, 2004.
(2) Diamond, D. *Principles of chemical and biological sensors*; Wiley: New York, 1998.
(3) Taylor, R. F.; Schultz, J. S. *Handbook of chemical and biological sensors*; Institute of Physics Publishing: Philadelphia, PA, 1996.
(4) Brodd, R. J.; Bullock, K. R.; Leising, R. A.; Middaugh, R. L.; Miller, J. R.; Takeuchi, E. *J. Electrochem. Soc.* **2004**, *151*, K1−K11.
(5) Gratzel, M.; Moser, J.-E. *Electron Transfer Chem.* **2001**, *5*, 589−644.
(6) Meninger, S.; Mur-Miranda, J. O.; Amirtharajah, R.; Chandrakasan, A.; Lang, J. H. *IEEE Trans. Very Large Scale Integr. (VLSI) Syst.* **2001**, *9*, 64−76.
(7) Tayhas, G.; Palmore, R. *Trends Biotechnol.* **2004**, *22*, 99−100.
(8) Lavin, P.; McDonagh, C. M.; Maccraith, B. D. *J. Sol-Gel Sci. Technol.* **1998**, *13*, 641−645.
(9) McDonagh, C. M.; Shields, A. M.; McEvoy, A. K.; Maccraith, B. D.; Gouin, J. F. *J. Sol-Gel Sci. Technol.* **1998**, *13*, 207−211.
(10) McDonagh, C.; MacCraith, B. D.; McEvoy, A. K. *Anal. Chem.* **1998**, *70*, 45−50.
(11) McDonagh, C.; Bowe, P.; Mongey, K.; MacCraith, B. D. *J. Non-Cryst. Solids* **2002**, *306*, 138−148.
(12) Cho, E. J.; Bright, F. V. *Anal. Chem.* **2002**, *74*, 1462−1466.
(13) Tang, Y.; Tehan, E. C.; Tao, Z. Y.; Bright, F. V. *Anal. Chem.* **2003**, *75*, 2407−2413.
(14) Cho, E. J.; Tao, Z. Y.; Tang, Y.; Tehan, E. C.; Bright, F. V.; Hicks, W. L.; Gardella, J. A.; Hard, R. *Appl. Spectrosc.* **2002**, *56*, 1385−1389.
(15) Cho, E. J.; Bright, F. V. *Anal. Chim. Acta* **2002**, *470*, 101−110.
(16) Davenport, M.; Titus, A. H.; Tehan, E. C.; Tao, Z.; Tang, Y.; Bukowski, R. M.; Bright, F. V. *IEEE Sens. J.* **2004**, *4*, 180−188.
(17) Cho, E. J.; Bright, F. V. *Anal. Chem.* **2001**, *73*, 3289−3293.
(18) Polerecki, L.; Hamrle, J.; MacCraith, B. D. *Appl. Opt.* **2000**, *39*, 3968−3977.
(19) MacCraith, B. P.; Lubos. WPO PCT Patent Application, 2002.
(20) Helf, S.; White, C. *Anal. Chem.* **1957**, *29*, 13−16.
(21) Ross, H. H. *Anal. Chem.* **1966**, *38*, 414−420.
(22) Stevens, B. US Patent 3,612,866, 1971.
(23) Malcolme-Lawes, D. J.; Warwick, P.; Gifford, L. A. *J. Chromatogr.* **1979**, *176*, 157−163.
(24) Jones, K.; Malcolme-Lawes, D. J. *J. Chromatogr.* **1985**, *329*, 25−32.
(25) Hobbs, S. E.; Hieftje, G. M. *Appl. Spectrosc.* **1995**, *49*, 15−19.
(26) Rinke, G.; Hartig, C. *Anal. Chem.* **1995**, *67*, 2308−2313.
(27) Burden, D. L.; Hobbs, S. E.; Hieftje, G. M. *Anal. Chem.* **1997**, *69*, 1936−1941.
(28) Chuang, H.; Arnold, M. A. *Anal. Chem.* **1997**, *69*, 1899−1903.
(29) Hobbs, S. E.; Potyrailo, R. A.; Hieftje, G. M. *Anal. Chem.* **1997**, *69*, 3375−3379.
(30) Burden, D. L.; Hieftje, G. M. *Anal. Chem.* **1998**, *70*, 3426−3433.

10.1021/ac048985g CCC: $30.25
Published on Web 12/13/2004

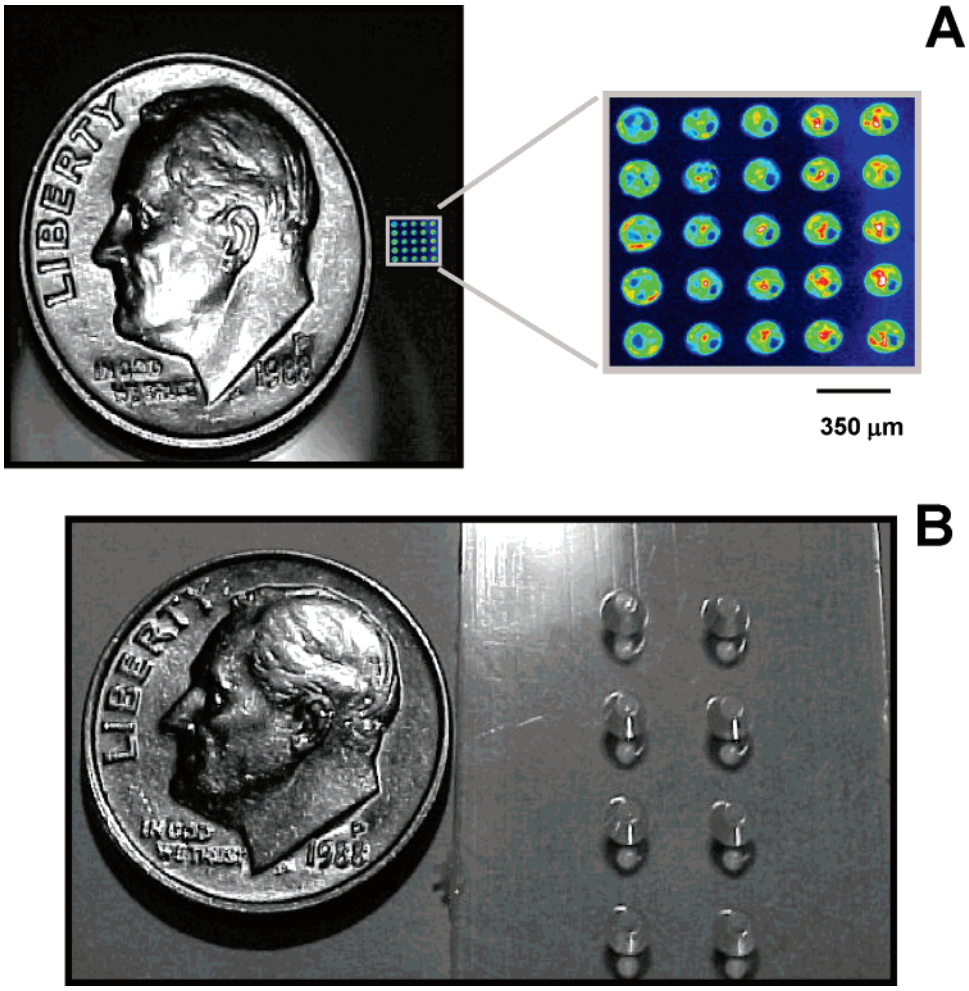

Figure 1. Images from a 5 × 5 pin-printed chemical sensor array (A) and a 4 × 2 array of frustrated conical pillars (B). A false color epifluorescence image of the 5 × 5 array is also shown in panel A. A U.S. dime is shown as a length scale.

process monitoring,[26] time-resolved fluorescence,[25,27,30,31,35] UV absorption,[34] steady-state fluorescence,[28,29,32,33,36,39,40] flow injection analysis,[37] and temperature sensing.[38] In comparison to a conventional light source, an RL light source is more simple, reliable, and compact, it is less prone to induce photochemical reactions, it exhibits a highly stable emission intensity,[21,34] and the RL per se requires no electrical power. To the best of our knowledge, there have not been any reports on the use of an RL light source in any sensor array format nor with more efficient light collection geometries (e.g., frustrated conical pillars).

The RL light source used in this research consists of a sealed β source (^{90}Sr) and a plastic scintillator. ^{90}Sr has a half-life of 28.5 yr, and it emits β particles with a maximum energy of 0.546 MeV.[41] ^{90}Y is a decay product of ^{90}Sr, emitting β particles with a maximum energy of 2.28 MeV and a half-life of 64 h.[41] As a β particle passes through the scintillator, it deposits energy in atoms and molecules along its path, creating excited atomic or molecular states through a nonradiative process. Radiative decay (luminescence) of these excited molecules produces numerous photons from each β particle. These photons can be used to excite other luminophores.

Luminophore quenching by O_2 depends on a variety of factors.[42] In the situation where luminophore molecules are sequestered within a homogeneous microenvironment and each luminophore molecule is accessed equally by the quencher molecules, quenching is described by the Stern−Volmer relationship:

$$\frac{I_0}{I} = 1 + K_{SV}[O_2] \qquad (1)$$

In this expression, I_0 and I represent the steady-state luminescence intensities in the absence and presence of O_2, respectively, $[O_2]$

(31) Burden, D. L.; Hieftje, G. M. *Rev. Sci. Instrum.* **1998**, *69*, 1595−1604.
(32) Chuang, H.; Arnold, M. A. *Anal. Chim. Acta* **1998**, *368*, 83−89.
(33) Chuang, H.; Arnold, M. A. U.S. Patent 5,708,957, 1998.
(34) Potyrailo, R. A.; Hobbs, S. E.; Hieftje, G. M. *Anal. Chim. Acta* **1998**, *367*, 153−157.
(35) Burden, D. L.; Hieftje, G. M. *Rev. Sci. Instrum.* **1999**, *70*, 50−57.
(36) Chuang, H.; Arnold, M. A. *Pure Appl. Chem.* **1999**, *71*, 803−810.
(37) Leach, A. M.; Burden, D. L.; Hieftje, G. M. *Anal. Chim. Acta* **1999**, *402*, 267−274.
(38) Leach, A. M.; Potyrailo, R. A.; Hieftje, G. M. *Anal. Chim. Acta* **2000**, *412*, 47−53.
(39) Reece, J. S.; Miller, M. J.; Arnold, M. A.; Waterhouse, C.; Delaplaine, T.; Cohn, L.; Cannon, T. *Appl. Biochem. Biotechnol.* **2003**, *104*, 1−11.
(40) Saarinen, M. A.; Reece, J. S.; Arnold, M. A.; Murhammer, D. W. *Biotechnol. Prog.* **2003**, *19*, 1335−1341.
(41) Browne, E.; Firestone, R. B.; Shirley, V. S. *Table of radioactive isotopes*; Wiley: New York, 1986.
(42) Lakowicz, J. R. *Topics in Fluorescence Spectroscopy*; Plenum Press: New York, 1991.

is the O_2 concentration, and K_{SV} is the dynamic Stern−Volmer quenching constant. K_{SV} depends on the luminophore's excited-state luminescence decay time in the absence of quencher (τ_0) and the bimolecular rate constant (k_Q), which describes the efficiency of collisional encounters between the luminophore and quencher:

$$K_{SV} = \tau_0 k_Q \quad (2)$$

For this ideal case, a plot of I_0/I vs $[O_2]$ will be linear with a slope (i.e., sensitivity) equal to K_{SV} and an intercept of unity. Models exist for other, more complex, scenarios.[42]

In the current work we determine the utility of an RL light source used in concert with a planar 5 × 5 multielement array and discrete sensor elements formed on the proximal face of plastic pillars with frustrated cone geometries. Toward these ends, we assess the analytical figures of merit for each sensor platform when it is excited by a He−Cd laser, an LED, or the RL light source. The sensor elements consist of an O_2-responsive photoluminescent molecule, tris(4,7′-diphenyl-1,10′-phenathroline)-ruthenium(II) ($[Ru(dpp)_3]^{2+}$), sequestered within a hybrid nanoporous xerogel.[13]

EXPERIMENTAL SECTION

Reagents and Materials. Tris(4,7′-diphenyl-1,10′-phenathroline)ruthenium(II) chloride pentahydrate ($[Ru(dpp)_3]Cl_2 \cdot 5H_2O$) was purchased from GFS Chemicals. It was purified according to the literature.[43] Tetraethoxysilane (TEOS) and *n*-octyltriethoxysilane (C8-TriMOS) were purchased from Gelest. Ethanol (200 proof ACS/USP grade) was obtained from Pharmco. Hydrochloric acid (ACS grade) was acquired from Fisher. Standard glass microscope cover slips were purchased from VWR. O_2 and N_2 gases were obtained from Irish Welding Supply. Navy blue spray paint (gloss, no. 1922) was manufactured by Rust-Oleum.

Unless otherwise noted, all chemicals and reagents were used as received without further purification. All water was treated with a Barnstead NANOpure II purification system.

Preparation of the $[Ru(dpp)_3]^{2+}$-Doped Sol−Gel-Derived Solution. The sol−gel processing solution was prepared by mixing, in order, TEOS (186 μL, 8.3×10^{-4} mol), C8-TriMOS (263 μL, 8.3×10^{-4} mol), EtOH (60 μL, 1.0×10^{-3} mol), 0.1 M HCl (50 μL, 5.0×10^{-6} mol), and 140 μL of 25 mM $[Ru(dpp_3)]^{2+}$ (dissolved in EtOH). This mixture was sonicated for 1 h, and then stored in the dark under ambient conditions before use.

PPCSA Fabrication. Figure 1A shows a photograph (left) and an epifluorescence image (right) from a typical 5 × 5 PPCSA. A U.S. dime is shown as a size benchmark. The PPCSA was formed on the face of a clean, glass microscope cover slip by using the aforementioned sol solution in concert with a MicroSys PA 5100 system (Cartesian Technologies) and a solid 200 μm diameter solid tungsten pin (Cartesian Technologies).

The standard method for forming a PPCSA has been described elsewhere.[12] In this approach a typical sensor element is ~1 μm in thickness. To ensure adequate signal-to-noise ratios from the PPCSAs under all experimental conditions, we produced 10 μm thick sensor elements by overprinting.

(43) Lin, C. T.; Boettcher, W.; Chou, M.; Creutz, C.; Sutin, N. *J. Am. Chem. Soc.* **1976**, *98*, 6536−6544.

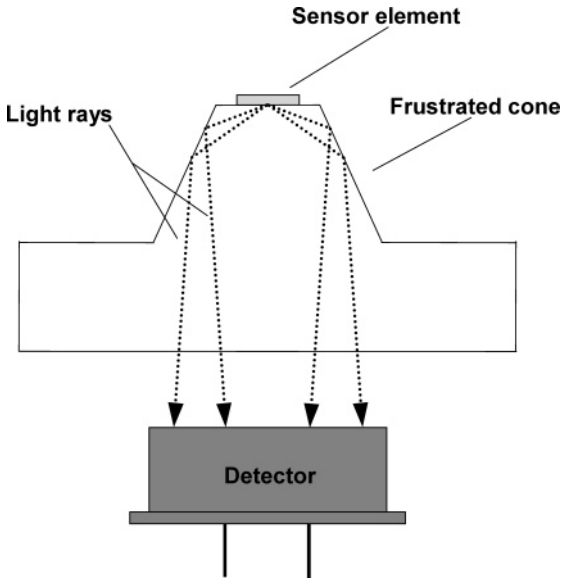

Figure 2. Cross section of the configuration facilitating improved efficiency of luminescence capture. The configuration exploits a frustrated cone located at the top side of the substrate.

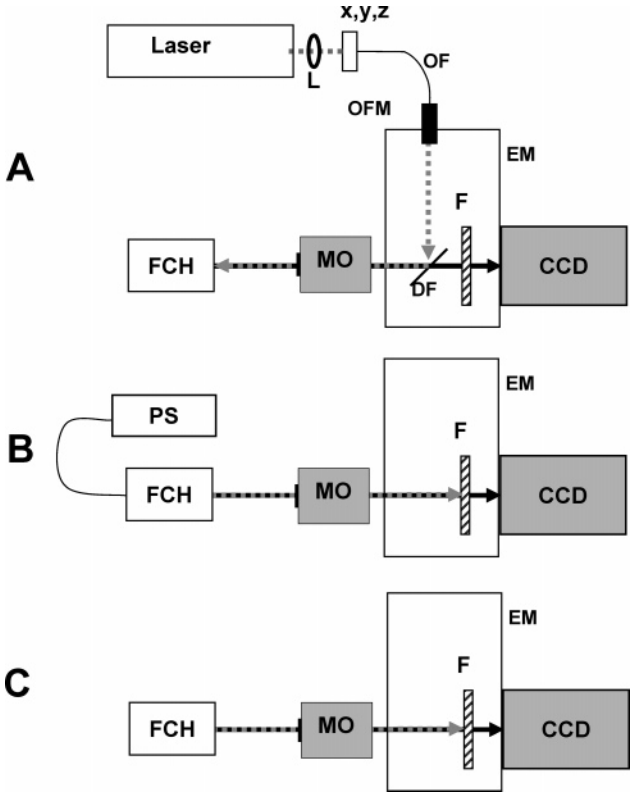

Figure 3. Simplified instrument schematics: (A) laser setup, (B) LED setup, (C) RL light source setup. Key: CCD, charge-coupled device; EM, epifluorescence microscope; F, long-pass optical filter; DF, dichroic filter; MO, microscope objective; FCH, flow cell holder; PS, power supply; L, lens; OF, all-silica optical fiber; x,y,z, precision *x*, *y*, *z* translation stage; OFM, custom optical fiber mount.

Sensor Elements on Frustrated Cone Pillars. Figure 1B shows a photograph of a typical 4 × 2 array of frustrated cone pillars made of poly(styrene).[18,19] A U.S. dime is again shown as a benchmark. Recent work by MacCraith et al. has led to the observation that a large fraction of the light emitted by a luminescent sensor element on a dielectric surface is propagated

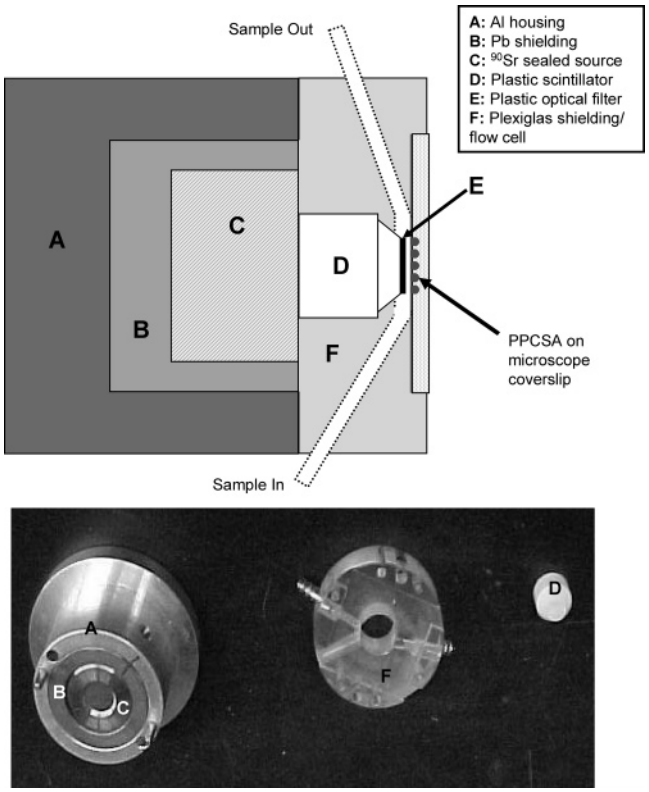

Figure 4. Schematic and photograph (semiexploded view) of the RL light source, flow cell, and sensor module.

into the substrate in a highly anisotropic manner and primarily at angles above the critical angle.[18,19] As a result, such light is not normally detected by conventional detection configurations. However, if the luminescent spot is located on the surface of an appropriately designed frustrated cone (frustum), the light radiated at high angles undergoes total internal reflection at the cone walls and is redirected downward toward an appropriately positioned detector (Figure 2). Such modifications of the substrate surface result in substantial enhancements of the detection efficiency (between 20× and 30×).

A single sensor element was formed on the proximal face of a frustum by using the aforementioned sol solution in concert with the pin printer and a 400 μm diameter solid tungsten pin (Cartesian Technologies). The typical sensor element diameter was 500 μm. The thickness of these sensor elements was only 1 μm, 10-fold less in comparison to that of sensor elements in the PPCSAs.

Postproduction Treatment of the Sensor Elements. All xerogel-based sensor elements were aged at 60 °C in the dark for at least 5 days prior to characterization to ensure that the xerogel was fully formed.

Instrumentation. Figure 3 illustrates the optical systems that we used to assess the performance of each sensor platform (PPCSA or frustum). In each system many of the components are identical. For example, the microscope objective (MO; Olympus, 4×), epifluorescence microscope (EM; Olympus model BX-1), long-pass filter (F; Omega, $\lambda_{cut-on} = 565$ nm), and thermoelectrically cooled charge-coupled devices (CCDs, Princeton Instruments, model TE/CCD-1317-K with a model ST-138 controller, or Roper Scientific, model Cascade 512B) are the same. All CCD images were acquired, displayed, and processed using WinView/32 software version 2.4.8.7 (Princeton Instruments) or RS Image software version 1.9.2 (Roper Scientific) running on a personal computer.

Table 1. Light Source Characteristics

source	peak wavelength (nm)	FWHM[a] (nm)	output power[b]
laser	442	< 0.1	3.1 mW
LED	465	25	60 μW
RL	435	59	80 nW

[a] Full width at half-maximum of the spectral profile. [b] At the sensor element(s).

To ensure that all systems were compared in a fair, head-to-head manner, the He−Cd laser and LED were warmed for approximately 2 h before an experiment was initiated. The CCDs were allowed to stabilize for at least 30 min. The RL light source required no warm-up time.

The laser-based system (Figure 3A) consists of a He−Cd laser (Laser; Liconix, model 4220N, $\lambda = 442$ nm). The laser output is focused by an f/2 fused-silica lens (L; Oriel) into the proximal end of an all-silica optical fiber (OF) that is mounted on a precision x, y, z translation stage (x,y,z; Newport). The distal end of the excitation fiber is placed within a custom optical fiber mount (OFM) that is connected to the EM. The laser beam is reflected off the front face of a dichroic filter (DF; Omega) to the MO, illuminating the entire sensor platform. The sensor platform is mounted within a home-built flow cell holder (FCH). The resulting luminescence from the sensor platform is collected by the MO and passed through the DF, and any residual excitation from the laser is suppressed further by the F. The sensor platform emission is imaged by the CCD. With the TE/CCD-1317-K CCD, the typical CCD integration time for these experiments was 40 ms.

The LED-based system (Figure 3B) used a modified Nichia America LED (part no. NSPB520S) as the excitation source.[15,17] The planar LED face was coated with a thin layer (100 μm) of blue spray paint to attenuate the yellow/red-edge tail from the LED's optical ouptut.[15] These particular LEDs were chosen because they provided a compromise among fluence, spectral maximums and bandwidth, and directionality. The LED is powered by a low-voltage dc power supply (PS) (CIC, model PS-1930). With the TE/CCD-1317-K CCD, the typical CCD integration time for these experiments was 150 ms.

The RL-based system (Figure 3C) consists of a sealed 2 mCi ^{90}Sr source (AEA Technology, product no. SIF.1171) and a 1 cm thick EJ-208 scintillator (Eljen Technologies). The scintillator surfaces, save the portion facing the sensor platform, are coated with a reflective coating (Eljen Technology, EJ-510). The RL source is completely enclosed within a custom FCH. Figure 4 presents a schematic (top) and a photograph (bottom) of the source, FCH, and PPCSA. A colored plastic filter (Roscolux no. 69 Brilliant Blue) is placed between the scintillator and sensor platform to remove the yellow/red-edge tail from the RL light source's optical output. With the TE/CCD-1317-K CCD, the typical CCD integration time for these experiments was >5 min.

(*Note:* When assembled, the RL light source poses a minimal radiation hazard with a dose rate on contact of 3 mrem/h, dropping to less than 0.25 mrem/h at 0.3 m from the FCH. As a point of comparison, the average person in the United States is

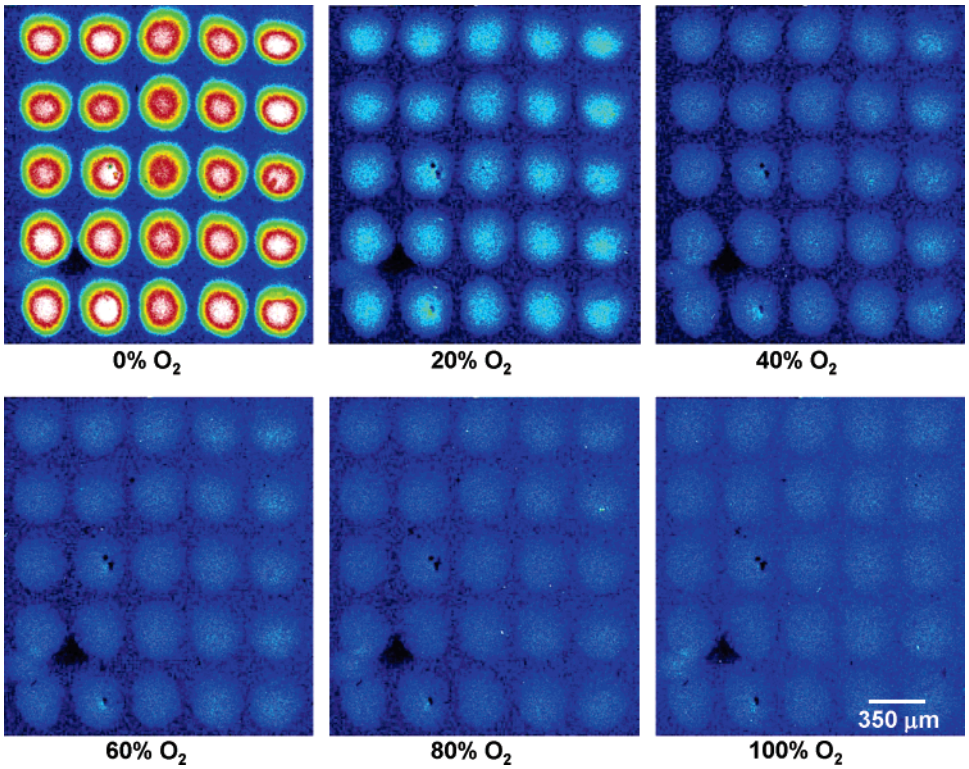

Figure 5. False color, O_2-dependent CCD images from a $[Ru(dpp)_3]^{2+}$-doped PPCSA excited with the RL source (10 μm thick sensor elements, 10 min integration time per image).

exposed to an effective dose equivalent of approximately 360 mrem (whole-body exposure) per year from all sources.[44] 10 CFR 20.1201 limits the maximum occupational dose for an adult to 5000 mrem (whole-body exposure) per year.)

Sample introduction to the sensor platform is carried out by using a home-built gas handling manifold that consists of two separate inlets that are controlled by individual flow meters (Gilmont Instruments, model GF 5542-1500). Each gas inlet is connected to a regulated gas cylinder containing either N_2 or O_2. All measurements were performed at room temperature.

RESULTS AND DISCUSSION

Source Characteristics. Several of the important characteristics of the three light sources are presented in Table 1.

PPCSA. Figure 5 presents a series of O_2-dependent false color CCD images from a 5 × 5 PPCSA excited by the RL light source. Under these conditions, the integration time for each image with the model TE/CCD-1317-K CCD was 10 min. One can clearly see the emission intensity decreases in step with the addition of O_2. Figure 6 presents the Stern−Volmer plots (i.e., calibration curves) for the PPCSA when it is excited by the laser, LED, and RL light source. Each datum represents the average response from the 25 individual sensor elements, and the error bars reflect the 99% confidence interval associated with the average values. The line passing through the data for each excitation source is the best fit to the Stern−Volmer expression (eq 1). *F*- and *t*-tests show that the recovered K_{SV} values were equivalent for all three excitation sources.

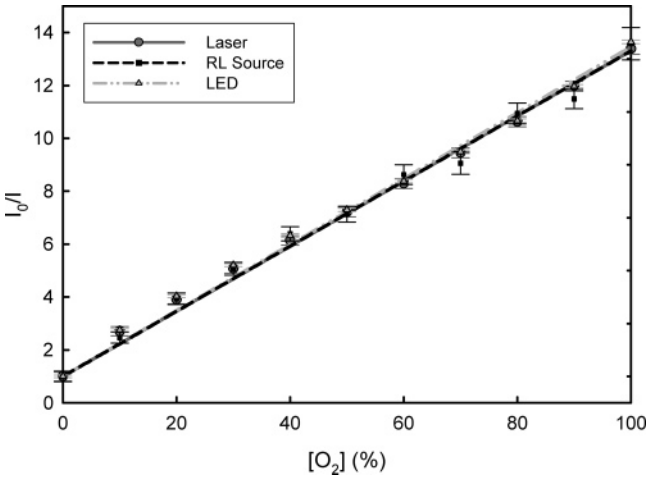

Figure 6. Comparison of the Stern−Volmer plots for a $[Ru(dpp)_3]^{2+}$-doped PPCSA excited with a He−Cd laser, an LED, and an RL excitation source. Lines represent the best fit to eq 1. Error bars represent the 99% confidence interval.

In a second series of experiments using the RL light source and PPCSA with the TE/CCD-1317-K CCD, we determined the response profiles (I_0/I vs $[O_2]$) as a function of CCD integration time (30 s to 10 min). The recovered K_{SV} values were integration time independent; however, the sensor's dynamic range was systematically compressed as the integration time decreased. That is, the full (0−100% O_2) calibration curves (not shown) rolled over to a progressively greater degree and at lower O_2 concentrations as the CCD integration time decreased. This problem arises from an inability to discriminate the weaker signals at higher quencher levels at the short CCD integration times. To address this issue, we repeated these experiments by using the more sensitive

(44) National Council on Radiation Protection and Measurements. *Ionizing Radiation Exposure of the Population of the United States: Recommendations of the National Council on Radiation Protection and Measurements*; NCRP: Bethesda, MD, 1987.

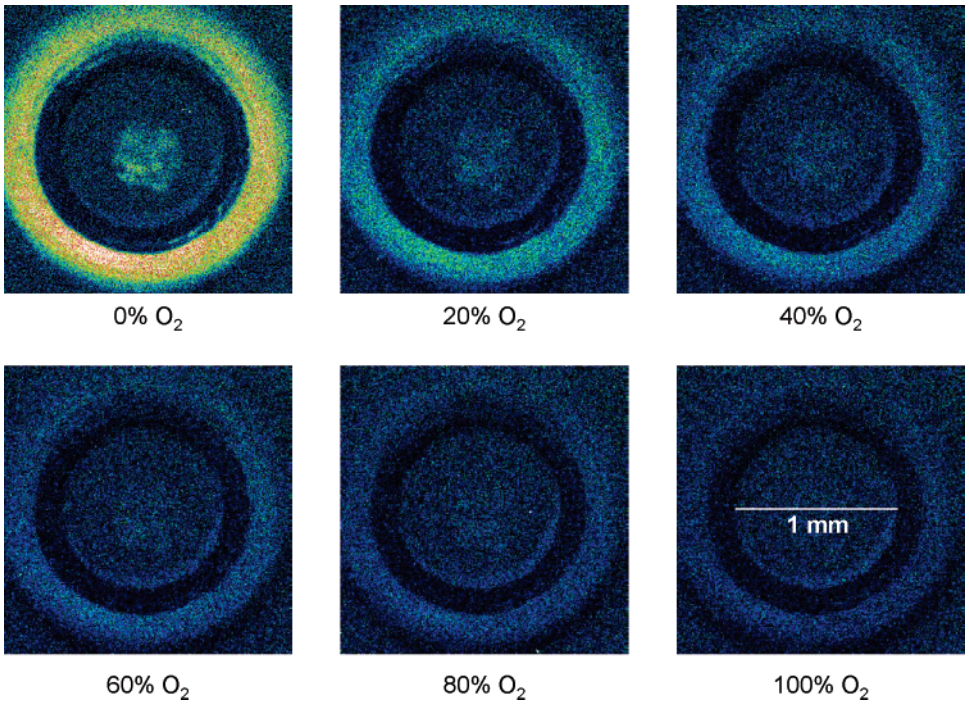

Figure 7. False color, O_2-dependent CCD images from a $[Ru(dpp)_3]^{2+}$-doped xerogel sensor element printed on a frustum platform excited with the RL source (1 μm thick sensor element, 15 s integration time per image).

Cascade 512B CCD. The observed results were identical to those shown in Figure 6 even down to 30 s integration times.

Frustums. One limitation that is made evident by our PPCSA results is that good analytical data can require substantial acquisition times with the RL source. This problem can, we showed, be partially alleviated by using a more sensitive CCD. Can we do better?

Figure 7 presents a series of O_2-dependent false color CCD images for a 1 μm thick sensor element on the proximal face of a poly(styrene) frustum when it is excited by the RL light source. The Cascade 512B CCD was used for these experiments. Despite the sensing element layer here being 10-fold thinner in comparison to the elements used in the PPCSA experiments, analytically useful images can be recorded with 15 s integration times. (*Note:* A series of experiments with a 10 μm thick sensor element on the frustum face showed that analytically useful images could be recorded with the RL light source even at 1 s integration times.) Inspection of Figure 7 shows that the emission intensity drops in step with the addition of O_2. One can also see that the signal intensity is much greater in the ring that surrounds the distal end of the frustum in comparison to the direct emission from the proximal frustum face where the sensor element is actually printed. In fact, the signal-to-background ratio in the ring is, at 0% O_2, 22-fold greater in comparison to the signal-to-background ratio from the proximal cone face.

The Stern−Volmer plots (not shown) for a 1 μm thick sensor element on a frustum excited by the laser, LED, and RL light source were equivalent to one another and yielded K_{SV} values that were equal to those shown in Figure 6.

CONCLUSIONS

The combination of a PPCSA with an RL light source is an attractive design for remote sensor array applications. The RL light source offers a compact alternative to conventional light sources that requires no electrical power. The main drawback of the RL light source is that data acquisition times can be long (~10 min). However, the integration of an RL light source with a frustum-based array and a higher sensitivity CCD allows one to construct sensor arrays that exhibit good analytical figures of merit with 1 s integration times.

ACKNOWLEDGMENT

We thank Gary Nottingham for assistance in the design and fabrication of the RL source and flow cell holder, and James Slawson for his assistance in radiation safety matters. The work at the University at Buffalo was supported by the National Science Foundation and the National Science Foundation Integrative Graduate Education and Research Traineeship (NSF IGERT) in Biophotonics. The Special EU Programmes Body (SEUPB), set up under the provisions of the Belfast Agreement (1998) for the EU Programme for Peace and Reconciliation in Northern Ireland and the Border Region of Ireland, provided funding for the work performed by the National Centre for Sensor Research at Dublin City University.

Received for review July 12, 2004. Accepted October 28, 2004.

AC048985G